THE ASTROPHYSICAL JOURNAL, 406:L71–L74, 1993 April 1

THE CIRCUMSTELLAR DENSITY DISTRIBUTION OF L1551NE

M. BARSONY
Harvard-Smithsonian Center for Astrophysics, MS-78, 60 Garden Street, Cambridge, MA 02138
AND
C. J. CHANDLER
Owens Valley Radio Observatory, California Institute of Technology 105-24, Pasadena, CA 91125
Received 1992 September 18; accepted 1993 January 13

ABSTRACT

We report the results of submillimeter photometry and 800 μm mapping of L1551NE, the second brightest Class I source in the Taurus dark clouds. Simultaneous modeling of the continuum spectrum and the azimuthally averaged 800 μm radial profile of L1551NE indicates a circumstellar envelope with a rather shallow density gradient [$\rho(r) \propto r^{-1/2}$]. Such shallow density gradients, although unexpected theoretically, have now been found around a number of other low-mass young stellar objects. We suggest that the magnetic fields in these sources may play a role in determining the observed density distributions.

Subject headings: ISM: jets and outflows — ISM: magnetic fields — stars: formation — stars: individual (L1551NE) — stars: pre–main-sequence

1. INTRODUCTION

The submillimeter spectral region is optimal for studies of protostars—objects enshrouded in relatively cool (10–50 K), dense ($n \geq 10^6$ cm^{-3}) gas and dust cocoons that are opaque even at infrared wavelengths, but become optically thin in the submillimeter. There are now four empirically defined phases of star formation, classes 0, I, II, and III. Class 0 sources are undetected at wavelengths shortward of 10 μm, but emit prodigiously in the submillimeter/millimeter wavelength range (André, Ward-Thompson, & Barsony 1993). Classes I, II, and III are distinguished by their spectral indices between the near and mid-infrared (e.g., Adams, Lada, & Shu 1987).

Through the modeling of both the continuum spectra of forming stars, and the spatial distribution of the intensity in the far-infrared/submillimeter, the density and temperature distribution of the circumstellar material on scales of 1500–2000 AU can be constrained (e.g., Ladd et al. 1991). Indeed, modeling of the Class 0 source, VLA 1623, shows that its spectrum is consistent with that of a central source heating a massive spherical dust and gas envelope extending out to 2000 AU, but with a density distribution flatter than that expected for free-fall (André et al. 1992).

A density distribution shallower than $r^{-3/2}$ is unexpected from the current theory of star formation (cf. Shu, Adams, & Lizano 1987), so to investigate whether this is also found on similar scales in the slightly more evolved, Class I, whose spectra are modeled as originating from large-scale ($\sim$0.1 pc) dust envelopes and small-scale ($\sim$100 AU) disks, we have mapped the second brightest Class I source in Taurus, L1551NE.

L1551NE was discovered by *IRAS* (Emerson et al. 1984). It is a highly embedded young stellar object in the nearby Taurus dark clouds (D = 140–160 pc), 0.4 north and 2.4 east of its famous neighbor, L1551-IRS 5. With a bolometric luminosity of $\approx 6\ L_\odot$, L1551NE is the second brightest Class I source in the Taurus dark clouds (after L1551-IRS 5). L1551NE lies toward the redshifted lobe of the large-scale molecular outflow powered by IRS 5 (Snell, Loren, & Plambeck 1980) and may be powering an outflow of its own (Moriarty-Schieven & Wannier 1991; Pound & Bally 1991). From broad-band optical polarization studies, L1551NE is known to be the illuminating source of a large ($\approx$2′) fan-shaped optical nebulosity (Draper, Warren-Smith, & Scarrott 1985). Such reflection nebulosities around Class I sources are the hallmarks of associated young, compact, molecular outflows (Barsony & Kenyon 1992; Moriarty-Schieven et al. 1992). A strong correlation between millimeter/submillimeter continuum emission strength and outflow activity has been noted as well (Cabrit & André 1991).

In this paper, we report results of submillimeter photometry and mapping of L1551NE. We use the dust radiative transfer code of Wolfire & Cassinelli (1986, 1987) to determine the density and temperature structure of the surrounding dust envelope and discuss the implications of our findings for current star formation modeling.

2. OBSERVATIONS AND RESULTS

The submillimeter and millimeter observations were made using the ^{3}He cooled bolometer UKT 14 (Duncan et al. 1990) on the James Clerk Maxwell Telescope (JCMT) on Mauna Kea, Hawaii, in 1991 September. Multiwavelength, single-point photometry was carried out from 2 mm to 450 μm, using a chop throw of 60″ in azimuth. Jupiter and Mars were used as primary calibrators, and W3(OH) and CRL 618 were adopted as secondary calibrators. The fluxes of W3(OH) and CRL 618 were determined through multiple observations of the planets and the secondary calibrators at the same airmass and sky opacity, which was monitored using the radiometer at the Caltech Submillimeter Observatory. The derived fluxes are listed in Table 1, together with the results for L1551NE. The uncertainties in the fluxes of W3(OH) and CRL 618 are standard deviations of the mean for all the observations carried out over a period of five nights and are dominated by errors in the calibration caused by the difference in the sky opacity between the observations of the planets and the sources. The pointing for L1551NE was checked using L1551/IRS 5. Combining our

TABLE 1

MEASURED FLUXES[a] FOR SECONDARY CALIBRATORS AND L155NE

λ (mm)	beam	W3(OH)	CRL 618	L1551NE
1.927.....	28″	5.3 ± 0.3	1.80 ± 0.30	<1.1 (3 σ)
1.260.....	21	9.8 ± 0.5	2.31 ± 0.24	0.80 ± 0.12
1.104.....	19	12.4 ± 1.1	2.59 ± 0.15	1.07 ± 0.11
0.790.....	16	29.5 ± 2.1	4.32 ± 0.38	2.22 ± 0.37
	13.5	23.3 ± 2.2	3.70 ± 0.44	1.75 ± 0.26
0.443.....	19	215 ± 50	15.3 ± 4.4	16.2 ± 4.9

[a] In janskys.

photometry with the *IRAS* fluxes (Emerson et al. 1984) results in the continuum spectrum shown in Figure 1.

Two oversampled, dual-beam maps of L1551NE were also made, using the diffraction-limited beam at 800 μm (13.″5 FWHM), by scanning the telescope in azimuth while chopping 40″. Both maps were 2′ × 1′, centered on $\alpha(1950) = 04^h28^m50^s.5$, $\delta(1950) = +18°02'09''$, and have 3″ pixel spacing. They were converted into single-beam maps using the NOD2 software (Haslam 1974), transformed into celestial coordinates, and co-added. The azimuthally averaged radial intensity profile of the 800 μm emission is plotted in Figure 2; the resulting map is shown in Figure 3 (Plate L4).

L1551NE is resolved in our 13.″5 beam, with a convolved source size of 16.″8 in RA and 18.″6 in declination. The geometric mean deconvolved source size is therefore 11.″4, corresponding to 2.4×10^{16} cm at the source. For comparison with the radiative transfer results below, we have fitted the continuum spectrum in Figure 1 with a single-temperature blackbody. The best-fit isothermal model of the 1.3 mm–60 μm photometry is depicted by the dotted line in Figure 1, and has parameters $T_d = 40$ K, $\tau_{800\,\mu m} = 0.005$, and a dust opacity frequency dependence of $\nu^{0.9}$ for our observed source size of 3.5×10^{-9} sr. For a mass opacity of $\kappa_{250\,\mu m} = 0.1$ cm^2 g^{-1} (Hildebrand 1983), this model predicts a mass for L1551NE of 0.05 $M_\odot$. This mass estimate is only for the object's circumstellar envelope, as we currently have no independent measure of the central object's mass. The sensitivity of the JCMT at 800 μm is ~30 Jy K^{-1}, so the flux observed in a 16″ beam also implies an optical depth of a few times 10^{-3} at 800 μm for $T_d = 40$ K, consistent with our spectral fit. A dust opacity frequency dependence of ν^2 resulted in extremely poor fits unless a high 800 μm optical depth was used, which was then two orders of magnitude too high to be consistent with the observed brightness temperature. The implied total extinction at optical wavelengths is ≈60 mag.

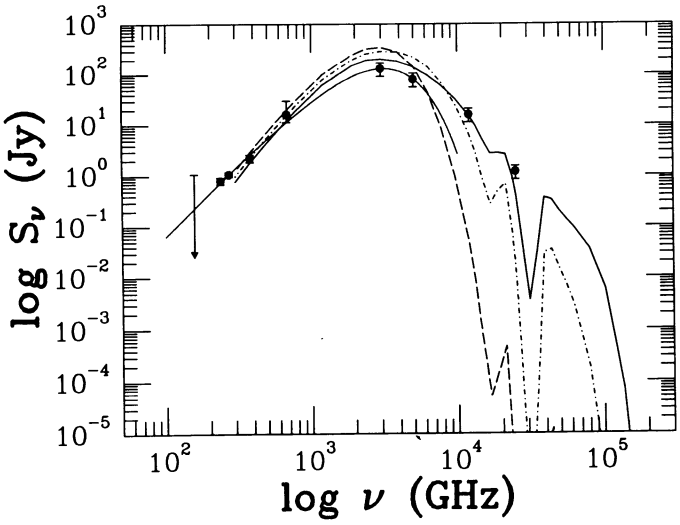

FIG. 1.—The measured continuum spectrum of L1551NE, with our model fits. The data points are from *IRAS* and our JMCT photometry. The 2 mm point is a 3 σ upper limit. The dotted line is an isothermal fit with $T_d = 40$ K, $\tau_{800\,\mu m} = 0.005$, and $\kappa_\nu \propto \nu^{0.9}$. The solid, dotted-dashed, and dashed lines represent WC models with density distributions varying with radius as $r^{-1/2}$, r^{-1}, and $r^{-3/2}$, respectively. These models are described further in the text.

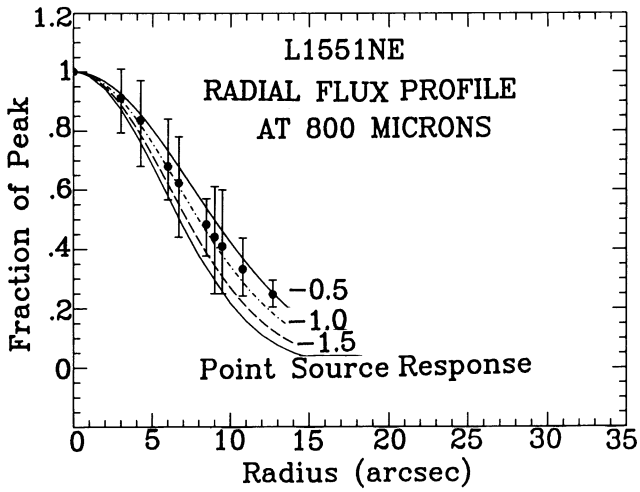

FIG. 2.—The azimuthally averaged 800 μm radial intensity profile of L1551NE. Error bars show the largest observed excursions of the data from the average value at each radius and reflect departures from spherical symmetry in the source. The dotted line represents the beam. The fits indicated by the solid, dotted-dashed, and dashed lines correspond to the WC models with $\rho \propto r^{-1/2}$, r^{-1}, and $r^{-3/2}$, respectively. The $\rho \propto r^{-1/2}$ provides the best *simultaneous* fit to the continuum spectrum and the 800 μm radial intensity profile of L1551NE.

Our 800 μm map of L1551NE is shown superposed on the optical image of the source in Figure 3. The lowest contours start to depart from circular symmetry, suggesting that at least some of the dust we detect may have been disrupted. Our submillimeter peak position is ≈3.″4 east of the published coordinates of the pointlike *R*-band source indicated by the arrow in Figure 3 (Campbell et al. 1988), but in view of the pointing uncertainty of the JCMT, we do not regard this difference to be significant.

3. DISCUSSION

3.1. *Modeling Results*

Since L1551NE is resolved at 800 μm, we have attempted to model its azimuthally averaged intensity profile at 800 μm and its continuum spectrum simultaneously with the dust radiative transfer code of Wolfire & Cassinelli (1968, 1987, hereafter WC). The dust properties used in this code are described in Churchwell, Wolfire, & Wood (1990). The effective frequency dependence of this dust mixture in the submillimeter/millimeter range most closely approximates a ν^2 emissivity law. There are five input parameters: the central source temperature, T_*, the source luminosity, L, the density power-law, q, $[\rho(r) \propto r^q]$, the envelope outer radius, r_{outer}, and the mass density at the outer radius, $\rho(r_{outer})$. The code then self-

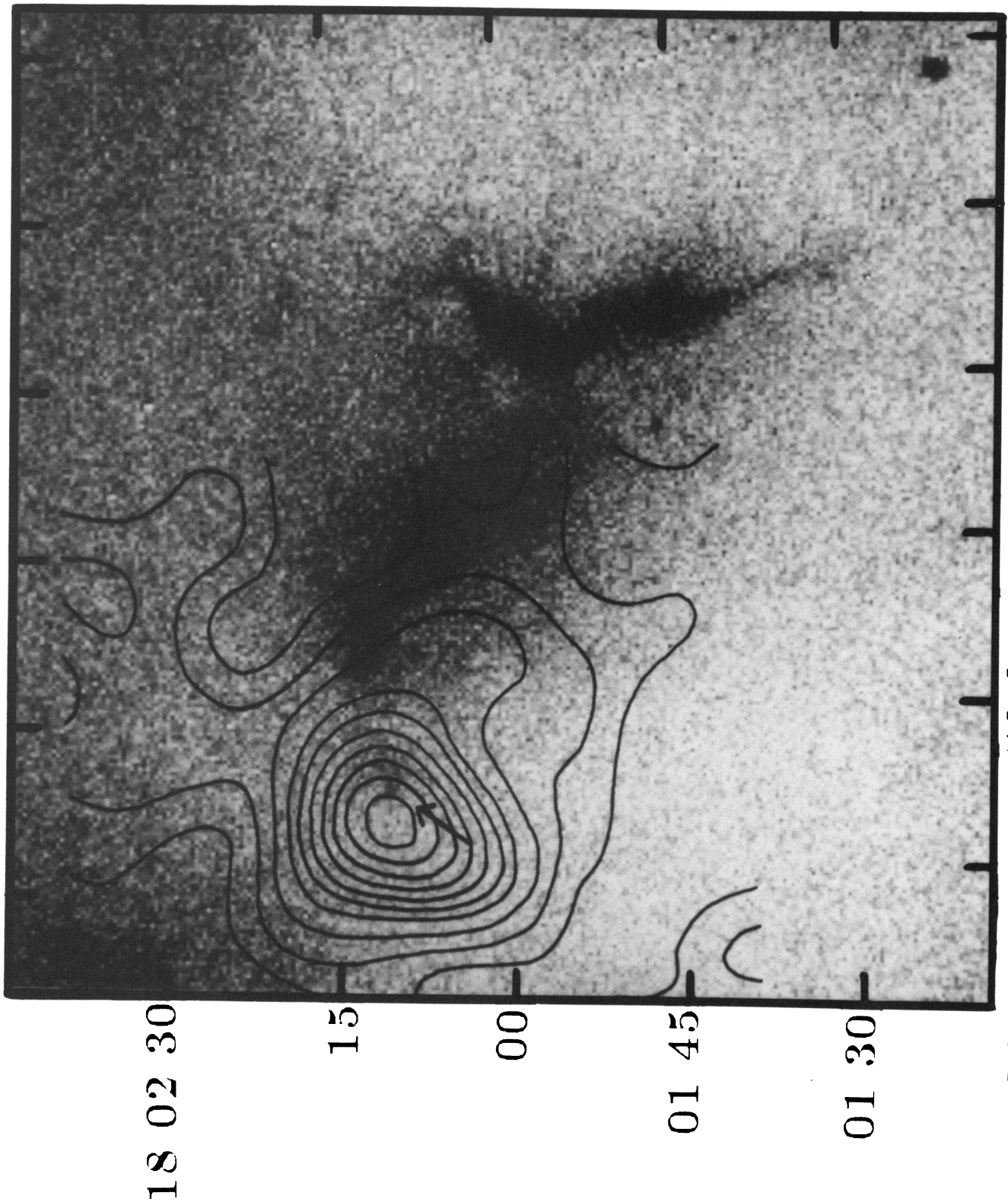

FIG. 3.—Our 800 μm JCMT map of L1551NE (*solid contours*) superposed on the 8000 Å image (Campbell et al. 1988) showing the associated optical reflection nebulosity. The arrow indicates the position of an optical knot previously identified with the *IRAS* source. The contour levels are at 1 σ intervals, where 1 σ = 0.17 Jy beam^{-1}.

consistently solves for the radial temperature distribution in the spherically symmetric dust envelope and produces a model of the resultant continuum spectrum and of the radial intensity distribution of the source at any desired wavelength.

Of the five input parameters, the luminosity and the outer radius are observationally constrained. Varying the central source effective temperature by a factor of 2 makes very little difference to the resultant SEDs or radial intensity profiles. The remaining parameters we are free to vary are the power law of the dust density distribution and the value of the mass density at the dust envelope's outer edge. The power-law of the dust density distribution is constrained by the radial intensity profile of the 800 μm emission (see Fig. 2). This leaves the value of the mass density at the envelope's outer edge as an unconstrained parameter. Varying this parameter has the greatest effect on the fit quality to the submillimeter/millimeter data points.

The code determines the inner radius of the spherical dust envelope self-consistently, assuming the grains melt at a specified temperature. Alternatively, the user may supply the code with a prescribed value for the inner radius of the dust envelope. In order to produce the best-fit WC model spectrum shown in Figure 1, we had to specify an inner "hole" to the dust envelope of 25 AU radius, otherwise models which would fit the submillimeter/millimeter points well would produce excess emission shortward of 100 μm.

The solid line of Figure 1 is our best-fit WC model to the continuum spectrum of L1551NE. The input parameters for this model were $T_* = 3500$ K, $L = 6\ L_\odot$, $\rho(r_{\rm outer}) = 1.21 \times 10^{-17}$ g cm^{-3} (corresponding to a gas number density of 5×10^6 cm^{-3}), $r_{\rm outer} = 1800$ AU, $r_{\rm inner} = 25$ AU, and a density power law, $q = -\frac{1}{2}$. Models with density power laws varying as r^{-1} and $r^{-3/2}$ are also shown in Figure 1 for comparison, by the dash-dotted and dashed lines, respectively. The 800 μm radial intensity profile of L1551NE and our best-fit WC model are plotted in Figure 2. Also plotted in Figure 2 are the WC models with $q = -1$ and $q = -3/2$, indicated by the dashed dotted and dashed lines, respectively.

As discussed by Ladd et al. (1991), the density distribution derived from continuum spectra is primarily constrained by the emission at near- and mid-infrared wavelengths. The 12 μm *IRAS* flux from L1551NE requires that there be a rather low column density of extinguishing material which, by fixing the outer density of the core, translates into the necessity for less material at smaller radii than would be obtained from the theoretically expected power law of $q = 1.5$–2. Because of this, the dust properties at long wavelengths have little effect on the derived density distribution (Natta et al. 1992).

The dust emissivity in the far-infrared/millimeter primarily affects the appearance of the continuum spectrum. The necessity for the isothermal model to have a dust emissivity with a shallow frequency dependence arises because of the width of the observed spectrum. In the WC model, the temperature and density gradients serve to broaden the emergent flux distribution, without the need to invoke an emissivity index less than 2. The effect of a lower emissivity index (and subsequently a higher submillimeter emissivity) would be to decrease the mass of dust needed to account for the flux at long wavelengths. Thus, the mass obtained from the isothermal fit is a lower limit. Possible explanations of how a shallow frequency dependence might arise are described by Beckwith & Sargent (1991).

3.2. *Shallow Density Distributions in Young Stellar Objects*

The density distribution we find for L1551NE is considerably flatter than that predicted for an infalling protostellar core, for which $q \geq -3/2$. Examples of shallow density distributions in dust envelopes have now been found around all masses of young stellar object (YSOs) (Churchwell, Wolfire, & Wood 1990 [G5.89−0.39]; Efstathiou & Rowan-Robinson 1992 [W3(OH), G32.806+0.192, G49.204−0.35, and G10.447+0.024]; Natta et al. 1992 [LkHα 198]; André et al. 1993 [VLA 1623]).

It is not clear what physical process causes the observed density distributions, although in low-mass objects three candidates are rotation, outflows, and magnetic fields. Rotation would seem to be ruled out in the case of the low-mass Class 0 source, VLA 1623, since its millimeter/submillimeter appearance on all scales down to 2″ is spherical, as opposed to rotationally flattened (André & Sargent, unpublished OVRO millimeter interferometer data). Since outflows are present in VLA 1623 and LkHα 198, and one is suspected to emanate from L1551NE (although mapping of this outflow at higher resolution and in the higher CO rotational transitions is needed), the outflows may have some role in establishing/influencing a YSOs circumstellar density distribution. However, the prototypical outflow source, L1551/IRS 5 is well modeled with an $r^{-3/2}$ density distribution (Butner et al. 1991).

A good candidate for providing extra support to the envelope is a magnetic field. Density distributions as shallow as $\rho(r) \propto r^{0.9}$ have been calculated as equilibrium states in clouds undergoing ambipolar diffusion (Lizano & Shu 1989), and the data presented here indicate that magnetic fields may be important for the support of material against gravitational collapse even on circumstellar scales. In this context, it is interesting to note that the protostellar source, IRAS 16293−2422, which also shows a rather shallow dust density distribution (Butner 1990), has recently been found to exhibit linear polarization at 1.1 mm of $2.8 \pm 0.5\%$ at a position angle of $144° \pm 5°$, indicating a magnetic field direction close to the minor axis of the flattened structure encompassing the embedded binary system (Tamura et al. 1992). Millimeter/submillimeter continuum polarization studies as probes of the magnetic fields surrounding embedded young stars have become routinely possible only recently, and L1551NE is one of the few low-mass YSOs strong enough in the submillimeter to allow measurement of its continuum polarization with current instrumentation.

We thank M. Wolfire for use of his dust radiative transfer code and for valuable comments. We would like to acknowledge PATT for granting JCMT observing time, and we thank "our supermarvelous, talented, creative, sexy, and bribable (for a price) telescope operator, Rusty," for his assistance during the observations. This work was completed during M. B.'s tenure as a postdoctoral researcher for the Smithsonian Astrophysical Observatory's Submillimeter Array Project. C. J. C. acknowledges the support of a SERC/NATO Fellowship.

REFERENCES

Adams, F. C., Lada, C. J., & Shu, F. H. 1987, ApJ, 312, 788
André, P., Ward-Thompson, D. & Barsony, M. 1993, ApJ, 406, 122
Barsony, M., & Kenyon, S. J. 1992, ApJ, 384, L53
Beckwith, S. V. W., & Sargent, A. I. 1991, ApJ, 382, 250
Butner, H. M., Evans, N. J., Lester, D. F., Levreault, R. M., & Strom, S. E. 1991, ApJ, 376, 636

Butner, H. M. 1990, Ph.D. thesis, University of Texas at Austin
Cabrit, S., & André, P. 1991, ApJ, 379, L25
Campbell, B., Persson, S., Strom, S. E., & Grasdalen, G. L. 1988, AJ, 95, 1173
Churchwell, E., Wolfire, M. G., & Wood, D. O. S. 1990, ApJ, 354, 247
Draper, P. W., Warren-Smith, R. F., & Scarrott, S. M. 1985, MNRAS, 216, 7P
Duncan, W. D., Robson, E. I., Ade, P. A. R., Griffin, M. J., & Sandell, G. MNRAS, 243, 126
Efstathiou, A., & Rowan-Robinson, M. 1992, MNRAS, in press
Emerson, J. P., Harris, S., Jennings, R. E., Beichman, C. A., Baud, B., Beintema, D. A., Marsden, P. L., & Wesselius, P. R. 1984, ApJ, 278, L49
Haslam, C. G. T. 1974, AAS, 15, 333
Hildebrand, R. H. 1983, QJRAS, 24, 267
Ladd, E. F., Adams, F. C., Casey, S., Davidson, J. A., Fuller, G. A., Harper, D. A., Myers, P. C., & Padman, R. 1991, ApJ, 382, 555
Lizano, S., & Shu, F. H. 1989, ApJ, 342, 834
Moriarty-Schieven, G., & Wannier, P. 1991, ApJ 373, L23
Moriarty-Schieven, G., Wannier, P., Tamura, M., & Keene, J. 1992, ApJ, submitted
Natta, A., Palla, A., Butner, H. M., Evans, N. J., & Harvey, P. M. 1992, ApJ, 391, 805
Pound, M. W., & Bally, J. 1991, ApJ, 383, 705
Shu, F. H., Adams, F. C., & Lizano, S. 1987, ARA&A, 25, 23
Snell, R. L., Loren, R. B., & Plambeck, R. 1980, ApJ, 239, L17
Tamura, M., Hayashi, S., Yamashita, T., Duncan, W. D., & Hough, J. H. 1992, ApJ, 404, L21
Wolfire, M. G., & Cassinelli, J. P. 1986, ApJ, 310, 207
———. 1987, ApJ, 319, 850